ISSN 0001-4370, Oceanology, 2010, Vol. 50, No. 2, pp. 149–165. © Pleiades Publishing, Inc., 2010.
Original Russian Text © Yu.D. Resnyanskii, M.D. Tsyrulnikov, B.S. Strukov, A.A. Zelenko, 2010, published in Okeanologiya, 2010, Vol. 50, No. 2, pp. 165–183.

MARINE PHYSICS

Statistical Structure of Spatial Variability of the Ocean Thermohaline Fields from Argo Profiling Data, 2005–2007

Yu. D. Resnyanskii, M. D. Tsyrulnikov, B. S. Strukov, and A. A. Zelenko

Hydrometeorological Research Center of the Russian Federation, Moscow

E-mail : resn@mecom.ru

Received September 17, 2008; in final form, November 13, 2008

Abstract—The means, variances, and three-dimensional spatial covariances of the ocean temperature and salinity anomalies in the upper 1400 m layer have been estimated using data of the Argo profiling floats from 2005 to 2007. The results of data processing suggest the continuation of general warming of the ocean waters noted in a number of papers based on earlier data. A pronounced geographical and vertical nonuniformity characterizes this warming but, as a whole, it is mostly distinct in the upper 100 m layer both in the tropics and midlatitudes. For the first time, the unique characteristics of the Argo observing system allowed us to obtain estimates of the spatial statistics for salinity field, which is difficult in such analytical treatment. In particular, it has been demonstrated that the spatial structure of salinity anomalies is similar to those of temperature, excluding the case of the near-surface layer.

DOI: 10.1134/S0001437010020013

1. INTRODUCTION

Knowledge of the statistical structure of oceanographic fields is needed primarily as a substantial element of probabilistic description of the climate system. If the latter is understood as a multidimensional distribution of probabilities of all relevant oceanographic fields in every site of the World Ocean, then the three-dimensional field of means and three-dimensional covariances make up exhaustive description of instantaneous distribution in the case of a multidimensional normal law. In spite of the fact that the authenticity of the hypothesis of multidimensional normality can be questioned (for example [16]), obtaining information on the first and second moments of distributions of actual oceanographic fields is a necessary step toward understanding and modeling their statistics.

The importance of means (climatic norms) of oceanographic fields is evident. The usefulness of understanding the spatial statistical structure of oceanic fields can be illustrated by the following simple example. Assume that we are interested in the variability of mean temperature $\langle T \rangle$ (heat storage) in a certain volume V of seawater rather than in variations of directly measurable temperature T. It is evident that the dispersion of spatial mean $\mathbf{D}\langle T \rangle$ is substantially dependent on the spatial covariability of the field under study. In the case of unit correlation (an infinitely large radius of correlation) within the given volume, we have $\mathbf{D}\langle T \rangle = \mathbf{D}T$, while in the opposite case of tending to zero correlation radius, we asymptotically come to $\mathbf{D}\langle T \rangle = \mathbf{D}TV_{\text{corr}}/V$, where V_{corr} is the integral correlation volume determined by analogy with a one-dimensional integral scale of correlation ([4], p. 204). When V_{corr} tends to zero, $\mathbf{D}\langle T \rangle$ tends to zero too, which sharply contrasts with the case of unit correlation whereby dispersion of the mean equals the pointwise dispersion. Hence, the fundamental role of spatial covariability is quite evident when analyzing the integral characteristics of changeability and, similarly, when dealing with the differential features such as dispersion of gradients of water temperature or salinity, etc.

Information on spatial covariations is necessary when retrieving the state of the ocean from empirical evidence, too. So, knowledge of the first and second moments suffices for obtaining the linear ocean state estimates, optimal in the sense of the quadratic mean, from the measurement. On the other hand, it is known [11] that even substantially nonlinear transformations of a probabilistic process exert a relatively weak influence on the correlation estimates so that it is admissible to believe in a certain stability of the *linear* estimates with respect to departures from (multidimensional) normality. Currently, four-dimensional data assimilation, which involves accumulation of data of earlier observations in the numerical forecast that, in turn, is used as the first approximation for assimilation of current observations, belongs to the most popular procedures. However, when starting a data assimilation system of this type or when the forecast proves to be inaccessible for different reasons, covariances are needed in terms of deviations from climatic means to serve as a first approximation in these cases. It is precisely this type of statistics that is the subject of our examination in the present paper. The developed procedure of statistical estimation can be used (which we are intending to do) for obtaining the estimates of spa-

tial covariances of fields of *forecast errors*. Note that tools of the theory of optimal linear estimation can be used (and are used) for solving problems of optimization of the observation grid (see, for instance, [13, 23, 24, 27]).

This paper is dedicated to the statistical structure of fields of temperature T and salinity S of water based on measurement data of the Argo profiling floats over three years (2005–2007). Both fields T and S are represented as deviations of climatic distributions, i.e., as monthly climatic data of the digital atlas WOA2001 [8, 25]. Such a representation corresponds to passing from initial fields to anomalies that are the most interesting information for studies in long-term variability of the ocean and for many applications, including accounting for the state of the ocean when preparing meteorological forecasts and predicting climate change.

2. BACKGROUND

Fairly representative data samples are needed in order to obtain statistically valid estimates. For instance, such samples are the basis for compiling the updated versions of the digital atlas of the World Ocean WOA-94, WOA-98, WOA-2001, WOA-2005 [8, 19; 22, 25], which involves the first and second one-point moments (respectively, the means and root mean square values) of thermohaline and hydrochemical fields of the seawater from the surface to the bottom. The atlas is based on the data set of deep-water measurements in the World Ocean, collected during the whole history of oceanographic observations from 1772 to 2001 for WOA-2001 [10] and to 2005 for WOA-2005 [9]. However, the major portion of the set belongs to the second half of the 20th century, so that climate, restored from the atlas data, is representative precisely for this period. Specifically, the studies in climatic changes in the state of ocean water are based on this data [20, 21]. Similar studies have also been conducted on the basis of the set of marine meteorological observations I-COADS (International Comprehensive Ocean–Atmosphere Data Set) that covers a period of more than two hundred years 1784–2002 [29].

As for the two-point moments, such as spatial covariance and correlation functions, their estimation requires a rather large volume of observations, performed almost simultaneously or at least during a sufficiently narrow time gap to neglect variability in time against the background of changes in space. Currently available estimates of the statistical structure of the spatial variability of water temperature in the ocean [23, 24, 26, 27] are based on XBT-measurements, covering a limited depth range (up to 400–500 m) and very unevenly distributed over the ocean. The XBT-measurements concentrate along the routes of ships of opportunity and, therefore, cover comparatively narrow bands. Information on the spatial variability of salinity is limited to mean climatic distributions (the atlases of WOA series) or to individual fields restored from oceanographic surveys.

Prospects of more comprehensive analysis of the statistical structure of the thermohaline field emerged owing to recent development of an observation network based on deployment of the system of Argo profiling floats [6]. The broader depth range provides observational data volume sufficient for calculation of two-point spatial statistics down to 1.5–2 km in depth. Data for estimating spatial changes in salinity come to knowledge. A much more uniform distribution of measurements over the ocean facilitates understanding of the geography of spatial variability.

3. DATA AT HAND AND PREPROCESSING

Use has been made of data on vertical distributions of temperature and salinity in the upper ocean layer (1500 m thick) obtained from January 1, 2005, to December 31, 2007, with the help of the Argo profiling floats. These data are available in nearly real-time mode. They are distributed via channels of the Global Telecommunication System (GTS) of the WMO and accumulated at special centers of Argo data storage facilities.

In addition to Argo data, the GST channels are used to distribute information on vertical profiles of temperature and salinity provided by other observational systems such as moored and drifting buoys with sensor chains, expendable bathythermographs XBT mainly from ships of opportunity, and CTD-probes deployed from research vessels.

We have confined ourselves to Argo data when compiling data samples for statistical processing. They amount to 80% of the total volume of relevant profiling data for the upper 500-meter ocean layer and to almost 100% at greater depths. Exclusion of data of other types (moored and drifting buoys, XBT, etc) insignificantly reduces the population of the resulting data sample but secures stricter homogeneity in hardware effects and geographic distribution.[1]

Materials from the digital atlas WOA2001 [8, 25] were used as climatic data. They involve the results of objective analysis of the average distributions of temperature and salinity of water at standard depth levels as well as RMS deviations of mean values for every calendar month in one-degree squares. Climatic means represent the fields specified at every oceanic node of a one-degree grid. In contrast to the means, the distribution of RMS values is sparse because they are available only at nodes of squares whose population from

[1] It was discovered in work [15], which deals with long-term temperature trends from global data over the years 1957–1996, that systematic positive bias relative to hydrological and CTD measurements is inherent to the XBT data. Accounting for this bias of 0.2–0.4°C resulted in an almost two-fold decrease in estimates of long-term changes of heat content in oceanic waters, starting from the 1950s (0.62 of the case when bias was neglected).

the archive data suffices for RMS calculation. The area of "blank spots" (poorly populated squares) increases with depth. At the level of 500 m depth, the "blank spots" occupy about 20% of the surface of the World Ocean and their area exceeds 50% at the 1000 m depth levels.

The initial data set included relevant variables measured at arbitrary depth levels with a vertical pitch from 1 to 200 m. The number of measurement levels in a vertical profile varied from 1 to 500 within the depth range of 0 to 1500 m. The preprocessing of our data involved primary check, generation of ten-day subsamples,[2] reduction of the data to a discrete set of depth levels using linear interpolation (21 levels from 10 m to 1400 m), and compiling so-called superobservations.

The primary check has provisions for removing the repeating data, observations of wrong geography (land-connected data), and outliers, i.e., the data deviating from seasonally dependent climatic means by a value exceeding $\pm 3\sigma_T^{\text{clim}}(\pm 3\sigma_S^{\text{clim}})$, where $\sigma_T^{\text{clim}}(\sigma_S^{\text{clim}})$ are depth-dependent RMS deviations of temperature and salinity, respectively, according to the data of atlas WOA2001. We have approximately estimated the values of σ_T^{clim}, σ_S^{clim} by means of averaging over every one-degree square of the World Ocean. When doing so, we treated only squares with at least six archived observations, available in atlas WOA2001 for any calendar month at a specified depth level.

The superobservations were obtained through averaging the observed data located within a circle of fairly small radius r. This is reasonable in order to reduce the small-scale (subgrid) noise, which cannot be resolved with the available observing grid, and to enhance the spatial homogeneity of a sample under study (see, for instance, [18]). Checking for the sensitivity of statistical characteristics to the length of r showed that their estimates are virtually independent of $r = 1$–10 km, and subsequent calculations have been performed at $r = 5$ km.

The volume of observations subjected to preprocessing and reduced to specified levels is virtually depth-independent in the layer from the surface to 900 m depth, but drops approximately two times at depths from 900 to 1400 m (Fig. 1a). The total volume of the data sample for the 2005–2007 period at upper depth levels made up 220 000–230 000 for the whole World Ocean and 60 000–70 000for every latitudinal zone 20°–65° N, 20° S–20° N, and 20°–65° S. The temperature and salinity samples are almost equal in volume because Argo buoys provide concurrent information on both quantities.

The increase in the number of observations from 2005 to 2007 reflects development of the Argo system (Fig. 1b). As scheduled, the number of operational Argo buoys in the World Ocean reached 3000 by November 2007 (see http://ioc.unesco.org/iocweb/docs/Argo-3000-press-release.pdf). As a result, the volume of a ten-day preprocessed data sample made up 2500 for the depth range 0–800 m and about 1500 at 1400 m depth.

4. STATISTICAL ANALYSIS PROCEDURES

The first and second moments of spatial distributions of oceanic fields of temperature and salinity, namely, their means and spatial covariances (dispersion inclusive), were the subjects of our analysis. We did not examine temporal covariances and cross-covariances. Here, we describe the procedure for estimating the spatial covariances, including estimation of dispersion of observational errors, and the technique for checking the statistical significance of the discovered deviations from climatic norms.

4.1. A model of observed anomalies

Analytical treatment was aimed at anomalies (deviations from the climatic norm) $\Delta_i^{obs} = \xi_i^{obs} - \xi_i^{\text{clim}}$. Here i means individual observation and runs all values corresponding to a specified depth level and region for the period in question, ξ designates the field of temperature or salinity, and upper indexes *obs* and *clim* point to observed and climatic values, respectively.

We use the following model for statistical analysis: the observed anomalies Δ_i^{obs} are readings of a spatial-temporal random field Δ^{obs}, which, in turn, is the sum of three mutually uncorrelated components: the "signal" proper Δ (the component resolvable by the observing grid), the small-scale "noise" (the component unrecoverable by the observing grid and usually considered as representativeness error), and measurement errors. We combine both types of errors as a unique error field Δ_n, so that $\Delta^{obs} = \Delta + \Delta_n$. Note that, by definition, the field of "noise" features zero spatial correlations at scales solvable by the observing grid. Our goal is statistical estimation of mean values and spatial covariances of the field of the "signal." We are dealing with anomalies; therefore, their means may be regarded as displacements because they characterize feasible changes in the climatic state. Subdivision of the dispersion of observed anomalies $D = \mathbf{D}\Delta_i^{obs}$ into

[2] Ten days is the typical duration of a full measurement cycle of the Argo profiling buoy. On completion of the cycle, the data of vertical profiling enter the communication channels. Varying the time gate from 3 to 10 days has revealed that the general structure of computed correlations depends only slightly on gate duration. Decrease of the latter results in growth of fluctuations due to decrease in the number of pairs of observations available for computing spatial correlations, and to the respective increase in the estimate dispersion. This means that time-dependence within the specified time gate does not exert a substantial influence on calculation of spatial correlations.

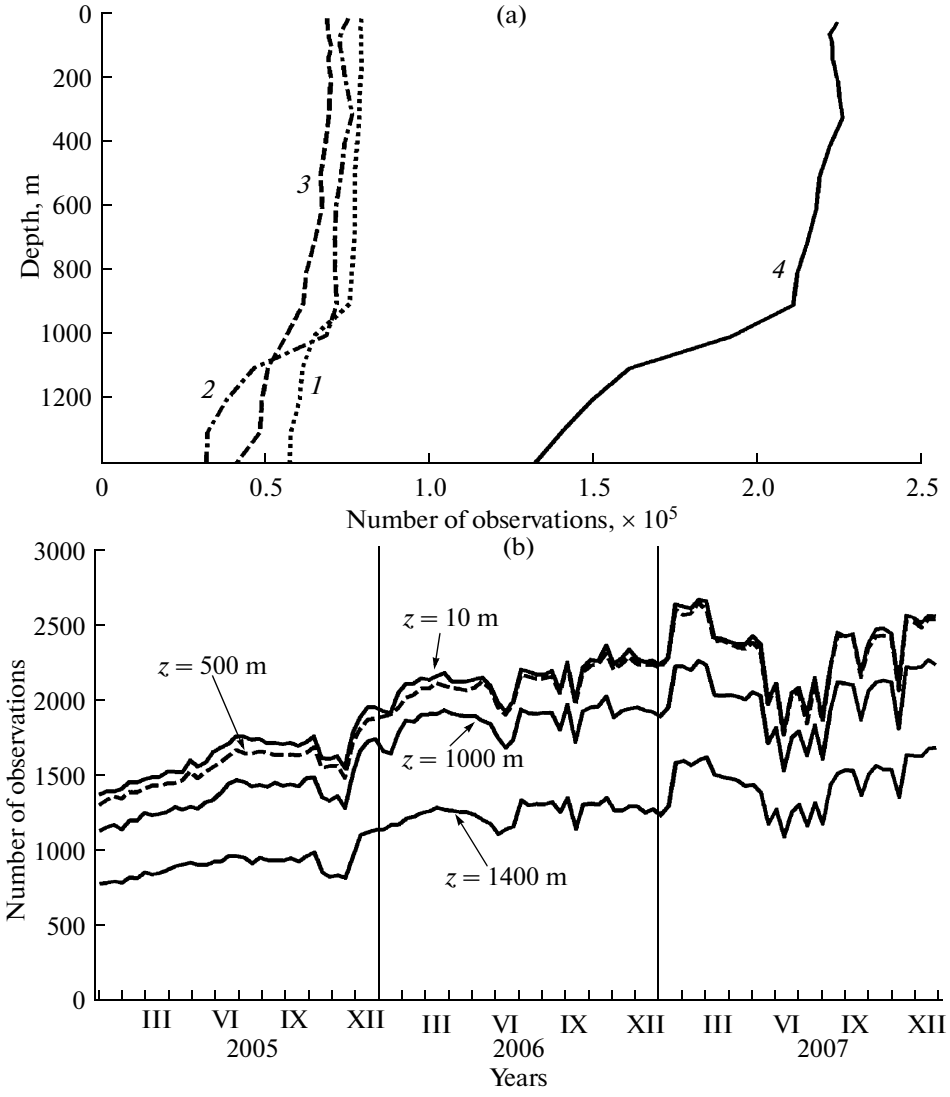

Fig. 1. Number of observations after preprocessing of data. (a) Depth dependence of total number for 2005–2007 period over three latitudinal belts and the World Ocean: (*1*) 20°–65° S, (*2*) 20° S–20° N, (*3*) 20°–65° N, (*4*) World Ocean (65° S–65° N). (b) Time-dependence of number of observations in ten-day data portions at fixed depths z from 10 to 1400 m in the World Ocean.

dispersion of "signal" and dispersion of "noise" will be given in section 4.4. We mark statistical estimates with the circumflex symbol.

4.2. One-point first and second moments

Based on the fact that the Argo buoys are almost evenly distributed over the deep-sea areas of the World Ocean ([7]), we estimate the means (displacements) and RMS deviations of anomalies Δ_i^{obs} for individual geographic regions using simple averaging over all available observations instead of probability-theoretical averaging. When doing so, we assume that zero mathematical expectation is inherent to the "noise" field, so that averaging of Δ_i^{obs} yields the desirable estimate of the mathematical expectation of the "signal" $\mathbf{E}\Delta$.

4.3. Spatial covariance functions

To obtain representative statistics from the available limited data volume, we introduce the assumption of the local (in boundaries of selected geographical regions, see below) *homogeneity* of field Δ; i.e., we suppose that covariances depend exclusively on offset $\mathbf{h}$ between a pair of points, the offset being understood as an element of rotation group SO(3) (to simplify the notation, we designate the "shifted" point $\mathbf{x}$ as $\mathbf{x} + \mathbf{h}$):

$$C^*(\mathbf{h}, z_k, z_l) = \mathbf{E}[\Delta(\mathbf{x}, z_k)\Delta(\mathbf{x}+\mathbf{h}, z_l)] - \mathbf{E}[\Delta(\mathbf{x}, z_k)]\mathbf{E}[\Delta(\mathbf{x}+\mathbf{h}, z_l)]. \quad (1)$$

Here, $\mathbf{E}$ is the operator of mathematical expectation, and indexes k and l designate numbers of levels. The nonnormalized covariance function is marked with an asterisk. For the sake of comparability of covariances

of different portions of the three-dimensional space of ocean waters, we compute the normalized (by anomalies' dispersion) covariance function as

$$C(\mathbf{h},z_k,z_l) = C^*(\mathbf{h},z_k,z_l)/D. \quad (2)$$

The normalized covariance functions are useful owing to their compatibility for different random fields and their realizations, similarly to the correlation functions. But, in contrast to the latter, they are more informative, being able to evaluate the "noise" contribution into the dispersion D (which we discuss below in item 4.4).

Like the one-point moments, the estimates of non-normalized covariance functions of temperature and salinity of water were calculated by substituting in (1) the averaging over all available observations with the assumption of horizontal statistical homogeneity instead of probabilistic averaging. The estimate of dispersion of an anomaly represents a sample dispersion $\hat{D} = \frac{1}{N-1}\sum_{i=1}^{N}(\Delta_i^{obs} - \overline{\Delta}^{obs})^2$, where N is the number of observations. In the first stage, use was made of an additional assumption concerning the horizontal isotropy of covariance functions, i.e., the independence of the offset $\mathbf{h}$ on its orientation. In the next stage, the anisotropy of function $C(\mathbf{h}, z_k, z_l)$ was estimated for several specified angles of the orientation of offset $\mathbf{h}$.

The calculations of covariance functions were made for $h = |\mathbf{h}|$ reckoned in the great circle arc from 0 to 300 km steps $\Delta h = 20$ km. Every computed value of the covariance function represented the average over the offset interval $(h - \Delta h/2, h + \Delta h/2$, the average being connected to the middle of the interval.

4.4. Estimation of dispersion of observational errors (noise)

The covariance functions allow us to estimate the dispersion of noise, defined above in item 4.1, for the case of mutually uncorrelated observation errors. The standard procedure [1] involves comparison of sample dispersion $\hat{D}$ of measured anomalies Δ_i^{obs} with the estimate of the value of their covariance function, extrapolated to the point of zero offset $\hat{C}^*(0)$. Covariance $\hat{C}^*(0)$ yields the estimate of the "signal" dispersion D_s. As already stated in item 4.1, dispersion D adds up to $D_s = C^*(0)$ and "noise" dispersion D_n. The latter, in turn, sums up the observational error dispersion D_m and representativeness error dispersion D_r: $D = C^*(0) + D_n \equiv C^*(0) + D_m + D_r$ [23, 28]. Note that the representativeness errors absolutely dominate in the case of the involved observations, based on Argo buoys system, because of the negligible instrumental errors of sensors of the system (for example, measuring platform PROVOR CTS3, being one of the types of Argo buoys, features measurement errors of temperature and salinity as low as ±0.002°C and ±0.003‰ according to http://www.ifremer.fr/dtmsi/anglais/produits/ marvor/provor_uk.htm).[3]

Thus, we are able to find the dispersion of noise $D_n = D - C^*(0)$ from quantities D and $C^*(0)$ and the "signal-to-noise" ratio as

$$\mu^2 = \frac{D_s}{D_n} = \frac{C^*(0)}{D_z} = \frac{C^*(0)}{D - C^*(0)} = \frac{C(0)}{1 - C(0)}. \quad (3)$$

Replacing the "theoretical" covariances in (1) with their sample estimates, we obtain the desired estimate of $\hat{\mu}^2$.

4.5. Estimation of statistical significance of observable deviations from climatic information

To interpret the displacements computed below and characterizing the mean deviations of climate, the sufficiency of the volume of empirical information "at hand" for trustworthy statements about *changes in climatic norms* must be established. In terms of the mathematical statistics, the hypothesis H (mathematical expectation $\mathbf{E}\Delta$ of the parent population, from which climatic anomalies Δ_i have been retrieved, differ from zero) must be tested for every depth level and region against the zero hypothesis H_0: $\mathbf{E}\Delta = 0$.

As a testing criterion of hypothesis H, we choose $|\nu| > c$, where

$$\nu = \frac{\overline{\Delta}^{obs}}{\hat{\sigma}_{\overline{\Delta}^{obs}}}. \quad (4)$$

Here $\overline{\Delta}^{obs} = \sum_{i=1}^{N}\Delta_i^{obs}/N$, and the horizontal line means averaging over all N observations within the analyzed domain G, $\hat{\sigma}_{\overline{\Delta}^{obs}}$ is the estimate $\sigma_{\overline{\Delta}^{obs}} \equiv \sqrt{\mathbf{D}(\overline{\Delta}^{obs}|H_0)}$, and c is a threshold value defined by the desired significance level α.

Let us consider the probability distribution of criterion ν starting from the displacement estimate $\overline{\Delta}^{obs}$ in the numerator in (4). Below, it will be shown that normalized empirical covariances reduces (everywhere excepting the only case of near-the-surface temperature which we neglect in our approximations) to the level 0.4 at the distance $R_{0.4} = 200 - 300$ km and virtually to zero at a distance $R_0 = 1500$ km (see below, Fig. 6). If we assume that the time-dependence of the examined anomalies is governed mainly by the large-scale water dynamics and that the characteristic velocity of oceanic currents makes up $U = 0.1$ m/s, then we can

[3] The indicated source of information on instrument precision, as is common in present-day sources in English, uses PSU (Practical Salinity Units) as the salinity units. They were introduced to facilitate comparison of salinity determinations from temperature and electric conductivity with water sample salinity estimation in pro mille units (‰). The values of salinity in PSU and pro mille units are fairly close. We use the latter in what follows.

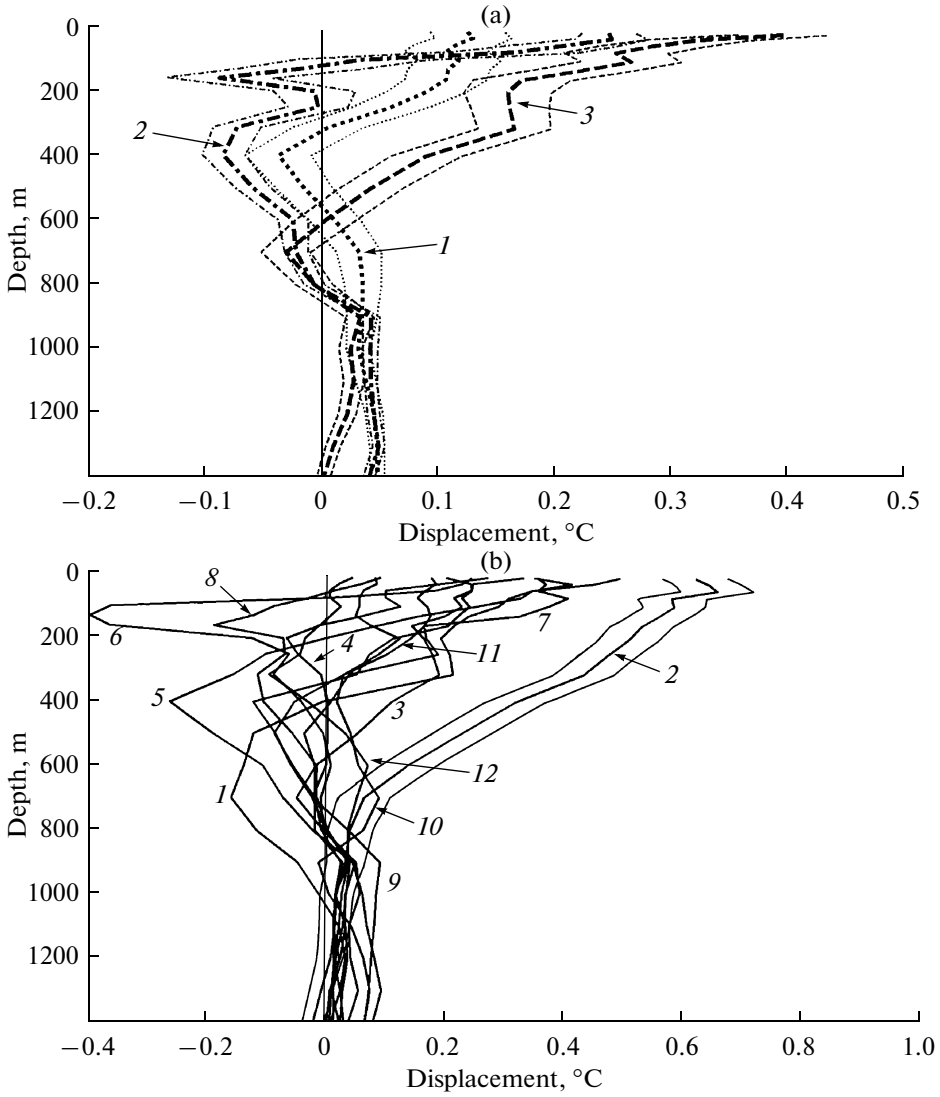

Fig. 2. Depth dependence of mean water temperature deviations of climate WOA2001 for the 2005–2007 period.
(a) Three latitudinal belts: (*1*) 20°–65° S, (*2*) 20° S–20° N, (*3*) 20°–65° N. Thin gray lines depict 95% confidence intervals of satisfiability of the hypothesis (*4*) at $n_{\text{eff}} \approx 2500$, $\hat{\mu}^2 = 4$. The hypothesis of nonzero mathematical expectation is acceptable if the vertical zero axis is outside these intervals.
(b) Twelve World Ocean regions marked with numbers as in the table. By example of the 2nd region: thin gray lines show the 95% confidence interval of satisfiability of the hypothesis (4) at $n_{\text{eff}} \approx 600$, $\hat{\mu}^2 = 4$. The typical width of this interval for other regions is 0.1–0.2°C in the layer down to 800 m decreasing to 0.02–0.05°C at the depths 1000–1400 m.

approximately recalculate $R_{0.4}$ and R_0 into the respective time-scales $T_{0.4} = R_{0.4}/U \approx 1$ month and $T_0 \approx 6$ months. These estimates show that covariances decay rather rapidly relative to the dimensions of the whole spatial–temporal domain. This allows us to apply the central limit theorem to the sequence $\{\Delta_i\}$ (for instance, [12]), so that the distribution of the mean $\overline{\Delta}^{obs}$ is approximately normal (even though individual anomalies significantly deviate from the norm). To compute the significance level of criterion (4), we need to know the distribution of $\overline{\Delta}^{obs}$ when the zero hypothesis is true. As it was clarified, this distribution is approximately normal and, by definition, $\mathbf{E}(\overline{\Delta}^{obs} \big| H_0) = 0$, while the dispersion will be determined below.

After ascertaining the probability distribution of the nominator in the criterion formula (4), let us address the denominator $\hat{\sigma}_{\overline{\Delta}^{obs}}$., which is a more complicated matter. The traditional estimation of standard deviation of the mean as $S/\sqrt{N}$, where S is the sample standard deviation of individual measurements and N is the sample population, is inapplicable here because

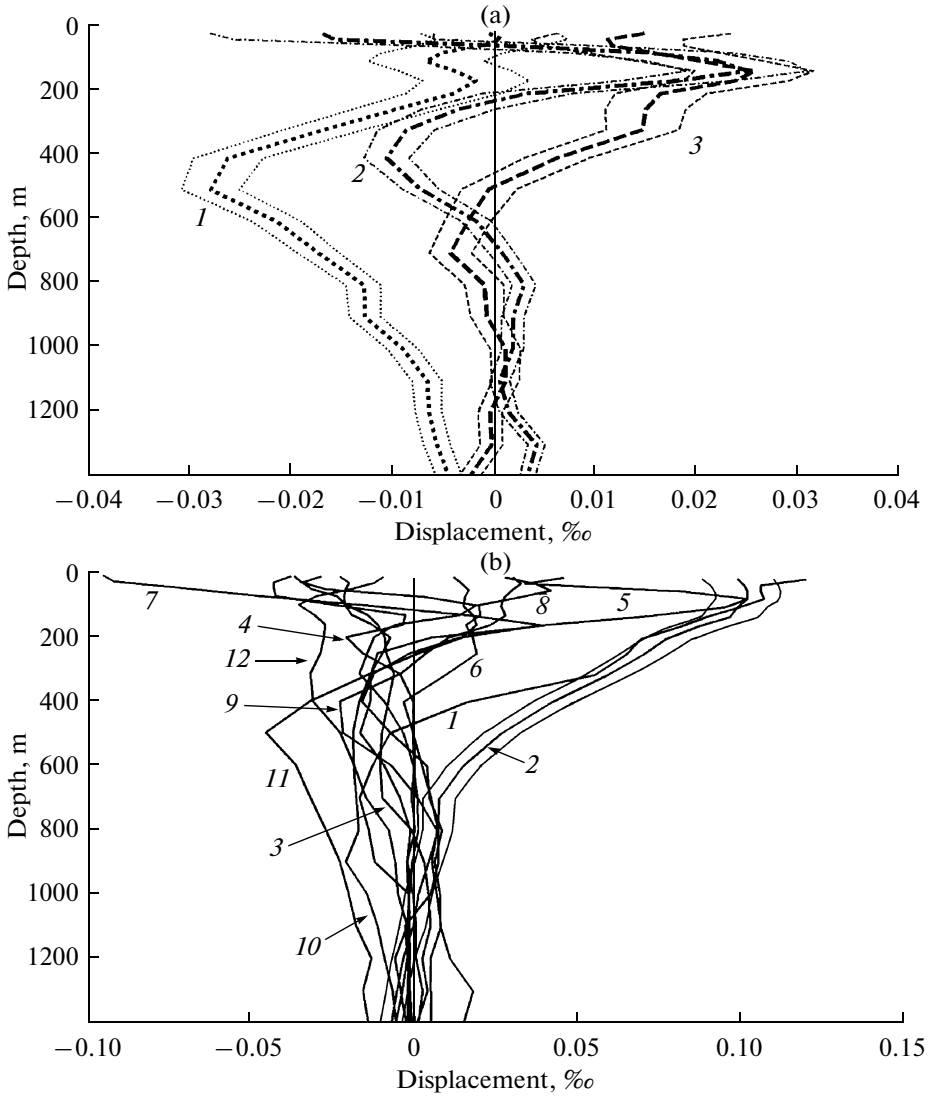

Fig. 3. Depth dependence of water salinity deviations from climate WOA2001 for the 2005–2007 period.

(a) Three latitudinal belts: (*1*) 20°–65° S, (*2*) 20° S–20° N, (*3*) 20°–65° N. Thin gray lines depict 95% confidence $\hat{\mu}^2 = 4$. The hypothesis of nonzero mathematical expectation is acceptable if the vertical zero axis is outside these intervals.

(b) Twelve World Ocean regions marked with numbers as in the table. By the example of the 2nd region: thin gray lines show the 95% confidence interval of satisfiability of the hypothesis (4) at $n_{\text{eff}} = 600$, $\hat{\mu}^2 = 4$. The typical width of this interval for other regions is 0.02–0.06‰ in the layer down to 800 m, decreasing to 0.005–0.010‰ at the depths 1000–1400 m.

of the substantial mutual correlation $\overline{\Delta}_i^{obs}$. We estimate $\sigma_{\overline{\Delta}^{obs}}$ approximately with the following assumptions:

(a) The "signal" field is homogenous and isotropic in the three-dimensional domain G (the geographic coordinates of given depth level and geographic zone correspond to the first and second dimensions while the third one is time) if $\mathbf{s}$ is defined as the vector (x, y, τ), where (x, y) are horizontal coordinates and $\tau = U t$.

(b) The covariance function of field $\Delta(\mathbf{s})$ is $C^*(\mathbf{w}) = D_s \exp(-|\mathbf{w}|/L)$, where $\mathbf{w}$ is the offset vector (the difference of two vectors that belong to the domain G), $|\mathbf{w}| = \sqrt{(x_1 - x_2)^2 + (y_1 - y_2)^2 + (\tau_1 - \tau_2)^2}$ is the magnitude of the vector, $L \approx R_{0.4}$ is a scale enabling us to approximate real horizontal covariances.

(c) Resolution of the observing grid suffices for approximate equality $\overline{\Delta}^{obs} \equiv \frac{1}{N}\sum \Delta_i^{obs} \approx \frac{1}{V}\int_G \Delta^{obs}(\mathbf{s})d\mathbf{s}$, where $V = A\ U\ T$ is the volume of domain G (A is the area of the involved ocean zone, T is the duration of the analysis making up three years).

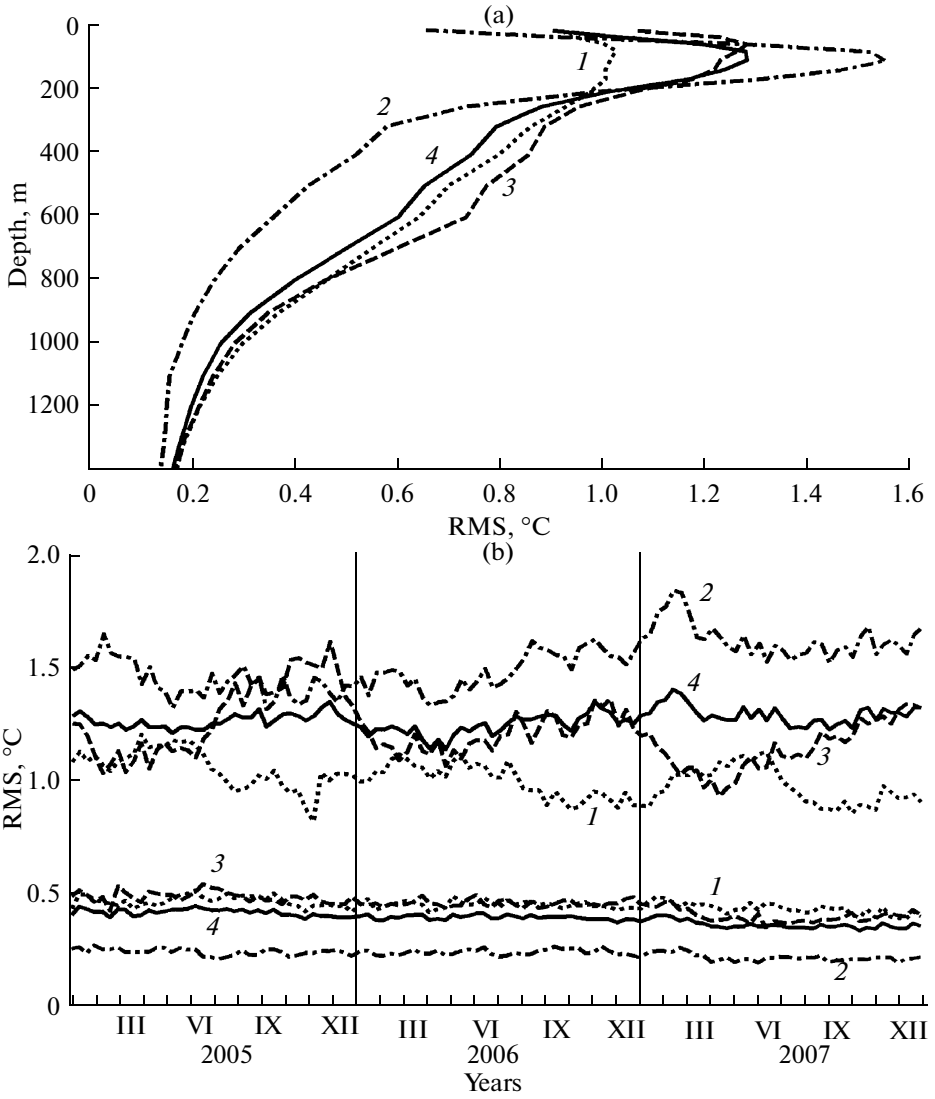

Fig. 4. Root mean square (RMS) deviations of water temperature (°C) from climate WOA2001 for the 2005–2007 period in three latitudinal belts and the World Ocean: (*1*) 20°–65° S, (*2*) 20° S–20° N, (*3*) 20°–65° N, (*4*) World Ocean (65° S–65° N).
(a) Depth dependence of the means over the above period;
(b) Time-dependence of RMS for ten-day data portions at the depth levels 100 m (upper curves) and 800 m (lower curves).

Under these assumptions and due to the statistical model introduced in item 4.1, the desirable conditional variance is

$$\mathbf{D}(\bar{\Delta}^{obs}\big|H_0) = \frac{1}{V^2}\int\limits_G\int\limits_G C^*(\mathbf{s}-\mathbf{u})d\mathbf{s}d\mathbf{u} + \frac{D_n}{N}.$$

Performing substitution $(\mathbf{s},\mathbf{u}) \longrightarrow (\mathbf{s},\mathbf{w})$, where $\mathbf{w}=\mathbf{s}-\mathbf{u}$, in the integral, we obtain

$$\mathbf{D}(\bar{\Delta}^{obs}\big|H_0) = \frac{1}{V^2}\int\limits_G d\mathbf{s}\int\limits_{G\mathbf{s}} C^*(\mathbf{w})d(\mathbf{w}) + \frac{D_n}{N}. \qquad (5)$$

Here $G\mathbf{s}$ designates the domain produced by differences $\mathbf{s}-\mathbf{u}$, where $\mathbf{s}$ is fixed while integration variable $\mathbf{u}$ runs the whole domain G. If, as it was assumed, the correlation radius of field Δ is much smaller than the dimensions of domain G, the internal integral in (5) may be approximated by a quantity independent of $\mathbf{s}$ and proportional to the so-called integral volume of correlation (see [4] too):

$$V_{\text{corr}} \approx \frac{1}{C^*(0)}\int\limits_G C^*(\mathbf{w})d\mathbf{w} \approx \frac{1}{C^*(0)}\int\limits_{R^3} C^*(\mathbf{w})d\mathbf{w}, \qquad (6)$$

where R^3 is a three-dimensional space containing domain G.

Then, since $C^*(0) \equiv \mathbf{D}\Delta(\mathbf{s}) \equiv D_s$, we finally obtain

$$\sigma_{\bar{\Delta}} = \sqrt{\mathbf{D}(\bar{\Delta}^{obs}\big|H_0)} \approx \sqrt{\frac{D_s}{N_{\text{eff}}} + \frac{D_n}{N}}, \qquad (7)$$

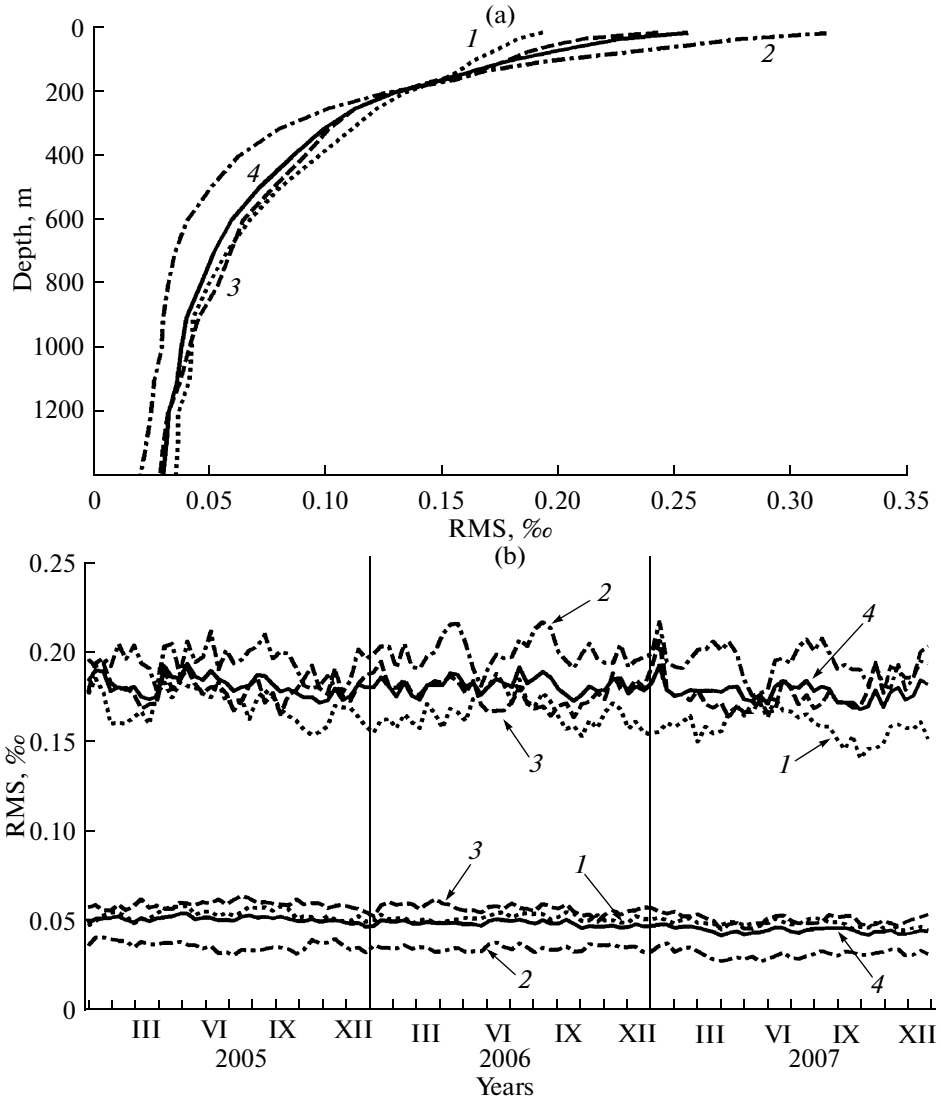

Fig. 5. Root mean square (RMS) deviations of water salinity (‰) from climate WOA2001 for the 2005–2007 period in three latitudinal belts and the World Ocean: (*1*) 20°–65° S, (*2*) 20° S–20° N, (*3*) 20°–65° N, (*4*) World Ocean (65° S–65° N).
(a) Depth dependence of the means over the above period;
(b) time-dependence of RMS for ten-day data portions at the depth levels 100 m (upper curves) and 800 m (lower curves).

where N is the number of measurements, μ^2 is the signal-to-noise ratio, determined from (3), and

$$N_{\text{eff}} = V/V_{\text{corr}} \tag{8}$$

is the efficient amount of *independent* observations of the same dispersion (D_s) as the signal Δ, correlated in time and space, the observations having a mean whose dispersion equals the dispersion of the mean $\overline{\Delta}$. It should be emphasized that derived formula (7) yields the estimate of dispersion of the spatial–temporal mean of anomalies $\overline{\Delta}^{obs}$.

Let us estimate N_{eff} in our case for the exponential covariance function. Substituting the exponential covariance function introduced above (see assumption (b)) into equation (6) and integrating it, we obtain

$$V_{\text{corr}} = \int_{R^3} \exp\left(-\frac{|\mathbf{w}|}{L}\right) d\mathbf{w} = 8\pi L^3. \tag{9}$$

With the correlation radius $L \approx 250$ km and the World Ocean area $A \approx 0.6 \times 4\pi a^2$ (a is the Earth's radius, coefficient 0.6 is the fraction of the Earth's surface that is occupied by the deep-sea ocean), formulas (8) and (9) give $N_{\text{eff}} \approx 7400$. Similarly, we derive $N_{\text{eff}} \approx 2500$ for every latitudinal zone and about $N_{\text{eff}} \approx 600$ for individual selected geographic regions. So, it is evident that although the total number of observations

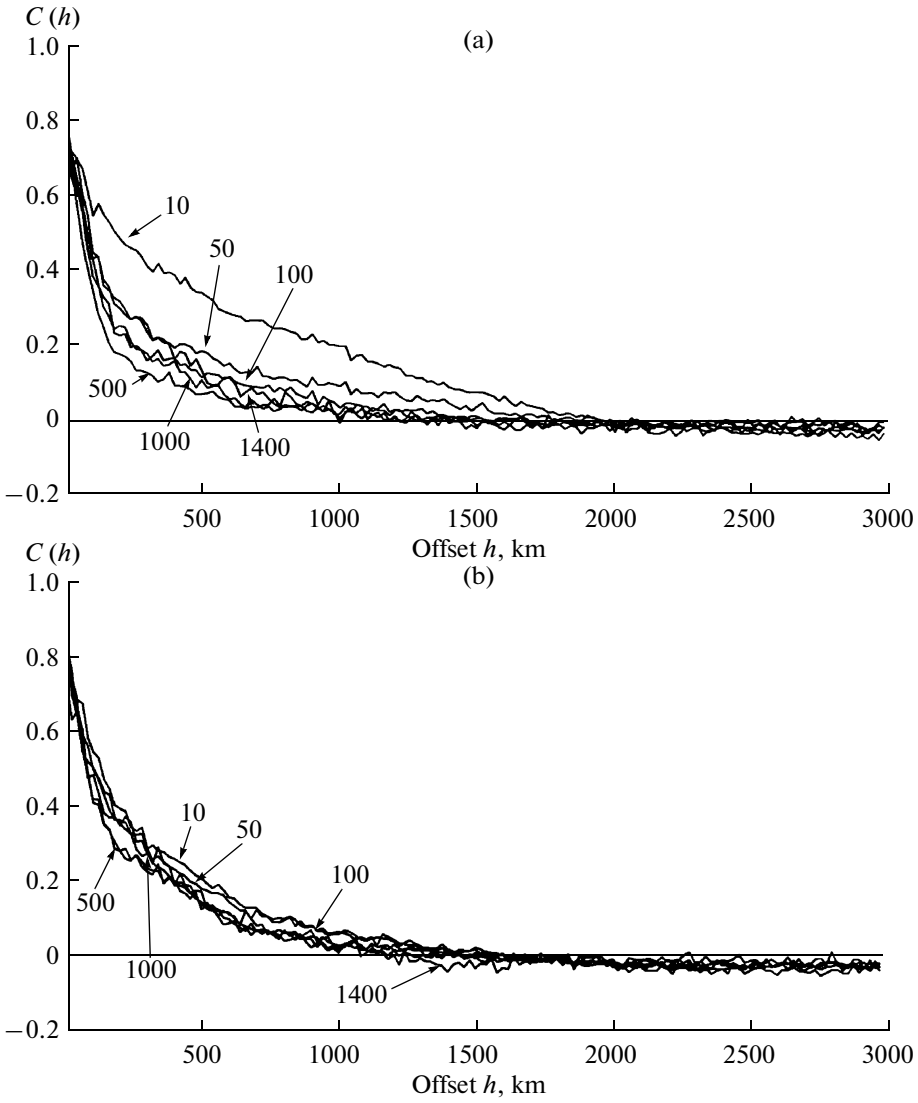

Fig. 6. The mean one-level covariance functions of displacements of water temperature (a) and water salinity (b) relative to climatic distributions, computed at the depths from 10 to 1400 m under the assumption of horizontal isotropy and averaged over 12 geographic regions (see table). Depths in meters are given at the curves.

amounts to hundreds of thousands, the equivalent number of *independent* observations is about ten thousand for the whole World Ocean and on the order of a thousand for every selected region. Nevertheless, in any case, this is a very large number and we can expect a high statistical significance of our inferences. In particular, we can estimate $\sigma_{\bar{\Delta}}$ quite precisely. Therefore, if hypothesis H_0 holds, statistics of criterion $\nu = \bar{\Delta}^{obs}/\hat{\sigma}_{\bar{\Delta}^{obs}}$ can be regarded as approximately equal to $\nu' = \bar{\Delta}^{obs}/\sigma_{\bar{\Delta}^{obs}}$, and, hence, normally distributed with zero mathematical expectation and unit dispersion: $\nu' \approx N(0, 1)$. This means that the threshold criterion value at significance level α can be obtained from the definition of the significance level:

$$\begin{aligned}\alpha &= P(|\nu| > c\,|H_0) \approx P(|\nu'| > c) \\ &= 2P(\nu' > c) = 2(1 - \Phi(c)),\end{aligned} \tag{10}$$

where Φ is the distribution function of the standard normal random quantity. Specifying $\alpha = 0.05$, we find $c = 1.96$ (for instance, [2]). *Ultimately, we reject the zero hypothesis on* $\mathbf{E}\Delta = 0$ *if* $|\bar{\Delta}^{obs}|/\sigma_{\bar{\Delta}} \geq 1.96$, *where* $\sigma_{\bar{\Delta}}$ *is defined by* (7).

Geography of estimation of statistics

No.	Data sampling area	Boundary coordinates (longitudes/latitudes)
1	Western North Atlantic Ocean	80°–40° W/20°–65° N
2	Eastern North Atlantic Ocean	40°–0° W/20°–65° N
3	Western part of Northern Pacific Ocean	120°–180° E/20°–65° N
4	Eastern part of Northern Pacific Ocean	180°–110° W/20°–65° N
5	Tropical Atlantic Ocean	70°W–15° E/20° S–20° N
6	Tropical Indian Ocean	34°–120° E/20° S–20° N
7	Western part of Tropical Pacific Ocean	120°E–160° W/20° S–20° N
8	Eastern part of Tropical Pacific Ocean	160°–70° W/20° S–20° N
9	Southern Atlantic Ocean	68°W–24° E/20°–65° S
10	Southern Indian Ocean	24°–146° E/20°–65° S
11	Western part of Southern Pacific Ocean	146°E–140° W/20°–65° S
12	Eastern part of Southern Pacific Ocean	140° – 68° W/20°–65° S

5. RESULTS OF STATISTICAL ANALYSIS

When finding the statistics, the World Ocean was subdivided into 12 regions: four in every latitudinal belt (see table). They have been chosen to be fairly small to apply the assumption of rough homogeneity but sufficiently large to secure representativeness of the sample within every region. In a number of cases, the statistics were evaluated for larger aquatic areas representing integration of the said regions such as zonal latitudinal belts or the World Ocean as a whole.

5.1. One-point statistics

5.1.1. Mean deviations of climate. Let us consider one-point statistics starting from displacements. Their vertical distributions are given in Figs. 2 and 3.

Positive displacements in the upper 100 m thick water layer is a common feature of all of the 12 selected regions (Fig. 2). Here and below we mention only those features of climate deviations that satisfy criterion (4) at the 95% significance level. These displacements reflect the warming of ocean waters during the examined three-year period (2005–2007) in reference to climate in WOA2001 retrieved from data of the preceding history of oceanographic observations. Statistically significant warming of the upper layer extends over all selected regions of the World Ocean. The largest displacements occur in the northern extratropic zone (0.4°C in the latitudinal zone 20°–65° N with the maximum 0.7°C in the eastern North Atlantic Ocean) and two-fold lower values occur in the southern extratropic zone (Fig. 2a). The tropical zone occupies an intermediate position in values of positive displacements of the upper layer water temperature between the north and south extratropics (0.25°C over the whole latitudinal belt with the maximum about 0.4°C in the western Pacific Ocean).

Climatic trends are extremely diverse in different ocean areas at the depths from 100 to about 900 m (Fig. 2b). Positive displacements dominate here, particularly the upper 100 m thick layer. Against this background, however, there are regions of explicit negative displacements. The latter concentrate mainly in the tropical latitudinal belt. The largest negative displacements have been discovered in the tropical Indian Ocean (minus 0.4 °C at 120 m depth) and the Atlantic Ocean (minus 0.25°C at 400 m depth). Displacements are mostly positive and weak at depths exceeding 900 m.

Salinity displacements exhibit similarly sophisticated distribution patterns (Fig. 3). Salinity growth, appreciable in recent years in extratropical regions from the surface down to 500 m depths, is accompanied by salinity decrease of the entire water column of 1400 m in the extratropical zone of the southern hemisphere (excluding the upper 200 m thick layer with insignificant deviations; Fig. 3a). However, trends of different signs occur in diverse oceanic basins of individual latitudinal zones.

In the northern extratropics, positive displacements (salinity growth) are observable in the Atlantic Ocean only (up to 0.1‰ near the surface, Fig. 3b). In the western part of this ocean, they extend to depths of 400 m and 700 m in the western and eastern parts of the ocean, respectively. As for the temperature, the eastern North Atlantic Ocean proves to be the most climatically "displaced" aquatic area (about 0.1‰ near the surface and virtually linear decrease to negligible values with depth down to the 700 m depth level). Negative (about 0.04‰) displacements of the mean salinity field are typical of the upper 200 m thick layer of the Pacific Ocean.

Different regions of the southern extratropics are dominated by negative displacements (Fig. 3b). However, the upper 200 m layer of the Atlantic sector and the western Pacific sector exhibits weak salinity growth (0.02–0.04‰) which passes into salinity decrease (down to minus 0.05‰ in the western Pacific Ocean) at depths below 400 m.

In the tropical zone, statistically significant positive salinity displacements occur in the layer from 50 to 200 m but they become negative at the depths 300–600 m. As for the whole World Ocean, positive significant displacements are characteristic of the upper layer of 300 m thick and of the layer of 800 to 1400 m with minor deviations between these layers.

Thus, our findings provide evidence of continuation of current total warming of ocean waters, which has been reported in a number of works based on empirical data for preceding years. This warming is characterized by explicit geographical inhomogeneity but, in total, is the most evident in the upper 100 m thick layer of any latitudinal zone.

5.1.2. Root-mean-square deviations. Figures 4 and 5 display the vertical distributions and time-dependence of the root-mean-square deviations of water temperature $\hat{\sigma}_{\Delta_T}$ and water salinity $\hat{\sigma}_{\Delta_S}$, as characteristics of variability of the respective fields.[4] In our case, the observable deviations of constant values indicate that our data series are not strictly time-independent (Figs. 4b, 5b). However, the relative variations of $\hat{\sigma}_{\Delta_T}$ and $\hat{\sigma}_{\Delta_S}$, are quite suitable to be acknowledged as acceptable for calculation of the generalized statistics for the whole period of three years. They do not exceed 10% in the main thermocline (lower clusters of curves in Figs. 4b and 5b). There is one and only one depth level of 100 m with the maximum of the vertical distribution of $\hat{\sigma}_{\Delta_T}$ where the relative changes of the latter in time do not exceed 20% upon averaging over the whole World Ocean and 49% over the tropical latitudinal zone. The respective estimates for salinity are 14% and 20%. For the temperature, the root-mean-square deviations are 4–5 times greater than the mean displacements. For the salinity, the mean and the root-mean-square values differ by more than an order of magnitude.

The occurrence of a local maximum at about 100 m depth is a distinctive feature of the vertical distributions of $\hat{\sigma}_{\Delta_T}$ (Fig. 4a), independently evidenced in [14], for example. Obviously, its origination is due to sharpening of vertical gradients within the seasonal thermocline typical of this depth range. Enhanced temperature variability is generated by seasonal processes in the course of which the seasonal thermocline at moderate latitudes appears in the spring and disappears after several months.[5] It is likely that the increased temperature variability is additionally influenced by the signal of synoptic eddies and internal waves, developing against the background of sharper vertical gradients independently of the latitudinal zone. The maximal thermocline $\hat{\sigma}_{\Delta_T}$ (about 1.5°C) occurs in the tropical zone. Here too, the most explicitly expressed vertical localization of higher $\hat{\sigma}_{\Delta_T}$ takes place due to the fact that the thickness of the main thermocline is at its minimum in the near-equatorial zone and grows with latitude φ according to the dependence $\sim \sin|\varphi|$ [3].

Such sharpening is absent in the distribution of salinity, and its root-mean-square deviations monotonically change with depth from 0.27‰ (on the surface of the whole World Ocean) or from 0.33‰ (on the surface of the tropical zone) to 0.02–0.03‰ in the 1000–1400 m layer (Fig. 5a).

5.2. Two-point statistics

5.2.1. One-level covariance function. Isotropic component. The covariance function, the other statistics remaining the same, changes from region to region due to the specific features of regional oceanographic fields. Let us consider the general properties of the depth-dependence of one-level (i.e., at $z_l = z_k$) covariances by the example of functions obtained by averaging individual covariance functions in every selected region and, therefore, characterizing the mean structure of horizontal covariances over the whole World Ocean (Fig. 6).

According to Fig. 6, the horizontal covariance scale decreases with depth from the surface down to about z_k = 500 m and increases from 500 to 1400 m. The gravitation of the horizontal scale minimum to a depth of about 500 m, where the core of the main thermocline with maximal vertical gradients occurs (see [3]), is attributable to the notion that this depth level is favorable for variations caused by synoptic eddies of the open ocean with the characteristic scale 10^2 km and, probably, by internal waves.

Except for the surface layer, the horizontal scales of temperature and salinity fields are roughly identical, which may be regarded as a consequence of the generality of the internal dynamic processes in the ocean that govern the variability of fields T and S in the water thickness. On the contrary, the structure of the surface layer (z_k = 10-50 m) is substantially conditioned by external forcings, such as surface fluxes of the momentum, heat, and fresh water. The structure of these

[4] The estimates of root-mean-square deviations σδT and σδS comprise the "signal" dispersion (real variability resolved by the observing grid) and noise dispersion making up 20–40% of the "signal" dispersion (see below, item 5.3).

[5] Deviations from the climatic means during transformations of the seasonal thermocline can be related to shifts in the timing of the emergence and destruction of the thermocline during specific years in reference to the long-period conditions.

fluxes, in turn, depends on the atmospheric conditions differently influencing the heat and fresh water transport from the atmosphere to the upper water layer. Here the salinity covariance proves to be shorter than the temperature one. Apparently, the mechanism of "refinement" of salinity anomalies is linked to the specificity of the structure of the field of atmospheric precipitation which is the main supplier of fresh water into the ocean surface layer. As is known, much stronger "patchiness" is characteristic of this field as compared with the atmospheric fields of wind and temperature influencing the surface temperature of the ocean.

As for the geographic dependence, the greatest variations of horizontal covariances from region to region occur in the upper layer. They decrease with depth, and, starting from the 200 m depth and as far as the lower boundary of the observation layer at 1400 m, the geographic dependence is weak against the background of fluctuations caused by the limited population of data samples (Fig. 7). In the subsurface layer, the most evident distinctions took place between the tropical and moderate-latitude ocean zones and between the west and east of the same zones. In the tropical zone, the covariances are longer due to zonal homogeneity of atmospheric forcings and to the effect of subequatorial currents of zonal orientation on the origination and transport of thermohaline anomalies. At moderate latitudes, the covariances prove to be shorter in the western sectors of the oceans compared to those in the eastern ones, apparently, because of narrow jet currents and associated eddies typical of the western oceans' boundaries at these latitudes.

5.2.2. Horizontal anisotropy. The anisotropy was estimated using calculation of the horizontal covariance functions for four orientations of the offset **h** with two diametrically opposed 45-degree sectors each. The perceptible distinctions in the orientation of covariance functions were found only for the zonal and meridional directions. The covariances for the directions from southwest to northeast and from southeast to northwest were virtually indistinguishable from the covariance computed for the assumption of horizontal isotropy. Therefore, we examine manifestations of anisotropy by the examples of covariances for zonal direction with **h** oriented within the angle range $\pm 22.5°$ relative to latitude and for the meridional direction with **h** oriented within the same range relative to the meridian (Fig. 8).

Like the other statistics, the anisotropy estimates depended on both geography and depth. The strongest anisotropy has been found in the tropical Pacific Ocean (Fig. 8a). The zonal scale of anomalies, defined as an offset at which $C(\mathbf{h}, z_k, z_l)$ drops to 0.05, makes up here about 3000 km, i.e., approximately six times as high as the meridional scale in accordance with the common idea of the structure of anomalies, the largest of which are conditioned by the El Nino phenomenon and extend in the zonal direction. The dominating orientation is observed in the upper water layer only. The thickness of the layer of strong anisotropy growth from 300 m in the eastern tropical Pacific Ocean to about 800 m in the west of the latter. The angular orientation disappears at the depths from 300 to 1400 m in the eastern sector of the layer under study and from 800–1400 m in the western one (Fig. 8b). It is notable that both hydrological fields, i.e., temperature and salinity, are similar in the anisotropy manifestations. This is an additional indication of the generality of physical processes determining the behavior and structure of these fields.

Other regions, including the tropical Atlantic and Indian oceans, exhibit much weaker zonal–meridional anisotropy. Anisotropy indications in the tropical Atlantic Ocean are not as distinct as in the Pacific regions and are traceable only in the upper 50 m thick layer. Such indications are hardly traceable in the tropical Indian Ocean. As for the extratropics, the anisotropy occurred in the upper 50 m thick layer of the northern Pacific Ocean only.

5.2.3. Vertical covariances. The vertical covariances, exemplified in Fig. 9, exhibit the following specific features. They are fairly "compact" in the upper layers, if the reference depth level z_k does not exceed 250–300 m, and broaden in the vertical with deepening of z_k. Compactness of upper layer vertical covariances is governed by the dynamics inherent to the ocean's active layer comprising the mixed layer and seasonal thermocline (pycnocline). Below the active layer, the dynamics of the main thermocline comes into force, which results in a greater characteristic vertical scale.

At zero horizontal offset, the approximate symmetry of covariance in the vertical takes place in reference to level z_k. In other words, the anomalies at a certain depth are equally correlated with anomalies at the upper and lower depth levels equally spaced away from the reference level. Such asymmetry with somewhat greater deviations is traceable at nonzero horizontal offsets h too. The covariances for temperature are more extended in depth (or more compact in the horizontal) than those for salinity. The only exception is the case of the most shallow reference level ($z_k = 10$ m) where the temperature covariances decrease with growing h faster than the salinity covariances.

5.3. Relationships of dispersions of "signal" and "noise"

The foregoing covariance functions make it possible to calculate the signal-to-noise ratio μ^2 using formula (3). Because of uncertainties inherent to the procedure of extrapolation of covariance function $\hat{C}(0)$, to the zero offset, the respective estimates of $\hat{\mu}^2$ are determined with a significant error and vary from 1.5 to 5.7 for $\hat{C}(0) = 0.6 - 0.85$ (Figs. 6–8). However, such a signal-to-noise ratio markedly exceeds the

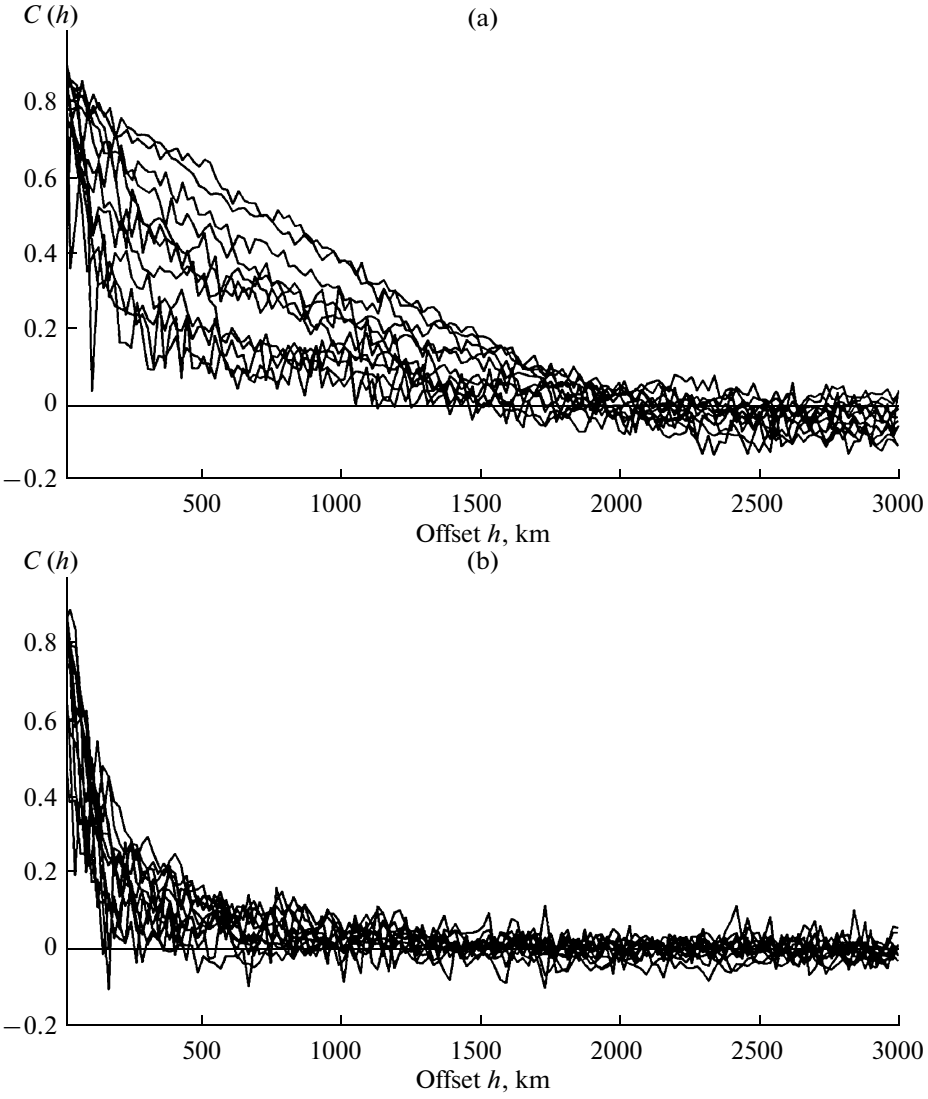

Fig. 7. One-level covariance functions of displacements of water temperature from climatic distributions, computed for 12 geographic regions at the depths 10 m (a) and 500 m (b) under the assumption of horizontal isotropy.

respective estimates from earlier works, dealing with the XBT-profiles. According to [27], $\hat{\mu}$ changed from 0.5 to 1.5 over the northern Pacific Ocean; according to [26], $\hat{\mu} \approx 1$ at any depth level down to 400 m; in [23], $\hat{\mu}$ from 0.5 to 2.9 are reported for different latitudes in diverse regions of the tropical Pacific Ocean with domination of estimates around unity and lower.

Thus, substantial improvement in the informativeness of modern Argo measurement system should be noted with respect to the XBT-profiling of past decades both in spatial coverage of the World Ocean and in the accuracy of the presentation of the observable variability of ocean waters. This was achieved at the expense of increased spatial–temporal resolution of the observing grid.

6. DISCUSSION

The observational data for the years 2005–2007, used to estimate the statistics, describe the current state of ocean waters. As follows from analysis of mean deviations, this state exhibits statistically meaningful positive displacements of water temperature relative to climate WOA2001, constructed from the data for the entire preceding history of oceanographic observations.

The indications of changes in the average state of ocean water, obtained from data for the foregoing three-year period, corroborate general trends emphasized in a number of works that, however, were aimed at earlier time periods. Our results provide evidence of the present-day continuation of general warming of waters noted in studies [20, 21]. The latter, relying

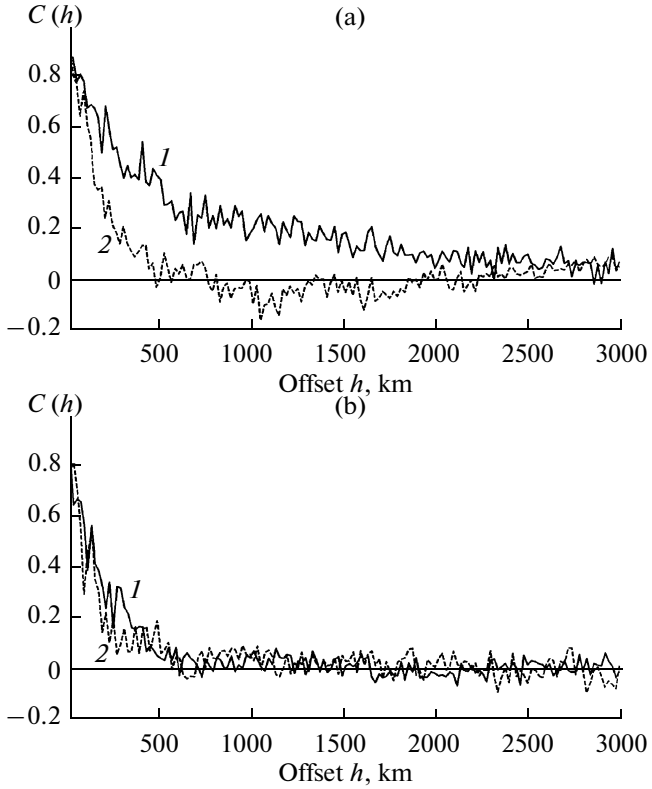

Fig. 8. One-level covariance functions of displacements of water temperature from climatic distributions, computed for depth levels 50 m (a) and 500 m (b) in the east of the tropical Pacific Ocean in the zonal (*1*) and meridional (*2*) directions.

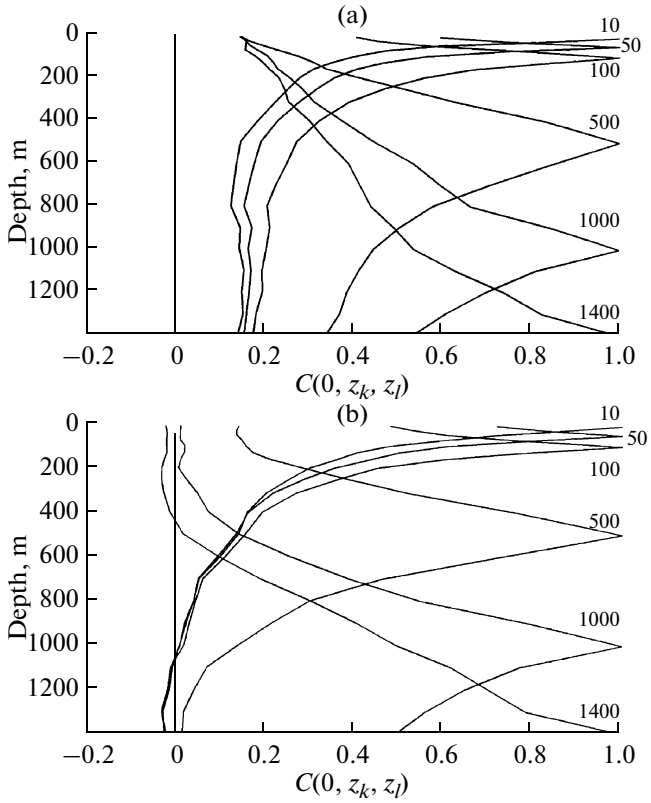

Fig. 9. Covariance functions of displacements from the climate of the water temperature (a) and the water salinity (b) averaged over 12 geographic regions (see table) and plotted as functions of depth z_l (vertical axis, m) at fixed horizontal offsets $h = 0$ and different reference depth levels z_k from 10 to 1400 m. The depth of reference levels in meters is given at the curves.

upon the information in databases of atlases WOA1998 [19] and WOA2001 [10], established trends of growth of heat storage in oceanic waters as deep as 3000 m observable during the last 50 years. In agreement with [21], we have found that the greatest warming takes place in the Atlantic Ocean, especially in its northern regions. The latitudinal–vertical distribution of mean changes agrees too. Particularly, the warming is at its maximum in the surface layers and attenuates with depth. The domain of water cooling in the meridional section is localized in the tropical zone at depth levels from 100 to 800 m.

Water warming is likewise indicated by the results of work [17] where changes in heat storage in the upper 1500 m thick layer of the North Atlantic Ocean within the latitudinal belt between 10°–70° degrees N have been studied from Argo buoy data for the years 1999–2005. According to [17], in spite of the positive temperature trends, displacement of heat storage of North Atlantic waters relative to the climate WOA2001 remained negative until 2005. However, by the end of 2005, this displacement is close to zero and, if the positive trend persisted during subsequent years, when data for our study was collected, this period had to become a period of positive displacements of temperature within the whole layer 1500 m thick relative to the climate WOA2001, which agrees with our results. The occurrence of a maximum of negative temperature displacements at the depth about 700 m, corresponding to the interface between the lower main thermocline and the upper intermediate waters, qualitatively agrees with our results too.

One more common feature is a distinct seasonal cycle of temperature anomalies at upper depth levels traceable from our data and from the results of work [17].[6] The occurrence of such cyclicity indicates that climate WOA2001 for the upper water layers (from 0 to 50–70 m) is not quite adequate in describing contemporary seasonal changes recorded with the Argo measurement system. Seasonal periodicity is most pronounced in the northern Atlantic and Pacific oceans

[6] By definition, anomalies are deviations of a seasonally changing climatic state. Their variability in time has to be deprived of seasonal periodicity if climatic data agree on average with the data of actual observations.

(the amplitude of temperature changes makes up 1.0–1.4°C at the depth 10 m). Seasonality indications are perceptible in changes in the salinity anomalies of the upper water layer in certain extratropical ocean zones (in the east of the North Atlantic Ocean, and in the south of the Indian and Pacific oceans). The discrepancies of our results and those of work [17] occur in the upper 100 m thick layer where both our estimates and data in [21] yield the greatest positive displacements, while negative deviations occur here according to the cited work. These disagreements can be attributable to differences in the time periods involved and, possibly, in data processing procedures.

The temperature displacements in the tropical Atlantic Ocean according to our estimates (0.07–0.10°C at depths of 900 to 1400 m) are also close to the temperature increase in intermediate waters of the equatorial zone of the North Atlantic Ocean (0.05–0.12°C from 500 to 1250 m depth), found from data in two zonal sections occupied in 1993 and 2000 [5].

As for the two-point statistics, the indications on the decrease of horizontal scales of temperature covariances from the surface down to 500 m depth, given above in item 5.2.1, agree with the findings of work [27] obtained on the bases of XBT-measurements in the North Pacific Ocean in 1968–1974 within the latitudinal belt 20°–50° N. In agreement with [27], our data indicate that the sharpest decrease in the horizontal scale occurs in the northern extratropical Pacific Ocean when passing from the near-surface layer ($z = 10$ m) to the underlying depth levels (about 50 m to the west and about 100 m to the east of this zone) and that thickness from 50–100 to 1400 m exhibits much weaker depth dependence of covariance horizontal scales. In agreement with [27], the covariance scale in surface waters, defined as the abscissa of the zero covariance function, makes up about 1600 km for the meridional direction and twice as much for the zonal one. In the tropical zone, the degree of anisotropy is relatively large because the dynamic structure of the zone is determined by a system of narrow currents of zonal orientation. As follows from our data, here the meridional scale is about 500 m while the zonal scale exceeds 3000 m (Fig. 8a). The six-fold difference in scales is close to estimates obtained in [23, 24] from XBT-observations in 1979–1983 in the tropical Pacific and Indian oceans (respectively, 300 and 1600 km with two-fold increase during El-Nino years). However, these data and those in [27] describe the upper 400 m layer giving no information concerning the structure of the underlying layers. We obtained such information after discovering earlier unknown weak growth of horizontal scales in the layer of 500 to 1400 m. Supposedly, this effect is due to the attenuation of synoptic disturbances below the core of main thermocline. Agreement with [27] is traceable too when comparing covariances for the eastern and eastern segments of the zone under study. In the west, the covariances prove to be shorter because of stronger development of the synoptic barotropic structures. Similar relationship is valid also for the west/east aquatic areas of the northern extra-tropical Atlantic ocean.

7. CONCLUSIONS

The estimates of first and second moments have been obtained for fields of temperature and salinity from observational data of Argo system. Among other, our analysis of the data provides evidence on presently continuing general warming of ocean waters reported in a number of works based of data for preceding years. The warming features the explicit geographic and vertical inhomogeneity but, in total, is the most pronounced in the upper 100 m layer both at tropical and moderate latitudes. Unique features of the observing system Argo made possible for the first time to obtain the estimates of spatial statistics of salinity field inaccessible to other research means. Specifically, it has been shown that spatial structure of the salinity field is similar to that of the temperature field, excepting the fields in the surface layer.

In the future, as Argo data accumulate, this analysis may be continued and refined. Nevertheless, the use of observations already available allowed us to obtain new important information concerning the statistical structure of thermohaline fields in the ocean, including refinement of the horizontal covariance structure in different geographic areas and earlier unknown evidence on vertical and three-dimensional covariances. This information and data processing procedures developed for its retrieval can be useful for improving techniques of analysis and assimilation of oceanographic data.

ACKNOWLEDGMENTS

The authors are grateful to the anonymous reviewer for helpful remarks concerning the initial version of the manuscript.

This study was supported by the Russian Foundation for Basic Research, project no. 08-05-13569-ofi_c and by Federal program "World Ocean," project 3 of subprogram ESIMO.

REFERENCES

1. L. S. Gandin, *Objective Analysis of Meteorological Fields* (Gidrometizdat, Leningrad, 1963) [in Russian].
2. G. Korn and T. Korn, *A Handbook in Mathematics* (Nauka, Moscow, 1978) [in Russian].
3. P. S. Lineikin and V. S. Maderich, *Oceanic Thermocline Theory* (Gidrometeoizdat, Leningrad, 1982) [in Russian].
4. A. S. Monin and A. M. Yaglom, *Statistical Hydromechanics* (Gidrometeoizdat, St. Petersburg, 1992), Vol. 1 [in Russian].
5. A. A. Sarafanov, A. N. Demidov, and A. V. Sokov, "On the Warming of Intermediate and Deep Waters in the

Equatorial North Atlantic," Meteorol. Gidrol., No. 3, 60–67 (2008).

6. Argo Science Team (D. Roemmich, O. Boebel, H. Freeland, B. King, P.-Y. Traon, R. Molinari, W. Brechner Owens, S. Riser, U. Send, K. Takeuchi, and S. Wijffels), "On the Design and Implementation of Argo—An Initial Plan for a Global Array of Profiling Floats," in *International CLIVAR Project Office ICPO Report No. 21. GODAE Report No 5* (GODAE International Project office, c/o Bureau of Meteorology, Melbourne, Australia, Le, 1998).
7. M. A. Balmaseda, A. Vidard, and D. L. T. Anderson, "The ECMWF Ocean Analysis System: ORA-S3," Monthly Weather Rev. **136** (8), 3018–3034 (2008).
8. T. P. Boyer, C. Stephens, J. I. Antonov, et al., World Ocean Atlas (2001).
9. T. P. Boyer, J. I. Antonov, O. Baranova, et al., "World Ocean Database 2005," in *NOAA Atlas NESDIS 60*, Ed. by S. Levitus (U.S. Government Printing Office, Washington, DC, 2006).
10. M. E. Conkright, J. I. Antonov, O. Baranova, et al., World Ocean Atlas (2001).
11. V. De Oliveira, "A Note on the Correlation Structure of Transformed Gaussian Random Fields," Austr. N. Zealand. J. Statist. **45**, 353–366 (2003).
12. P. Doukhan and G. Lang, "Rates in the Empirical Central Limit Theorem for Stationary Weakly Dependent Random Fields," Stat. Infer. Stoch. Proc. **5**, 199–228 (2002).
13. J. F. Festa and R. L. Molinary, "An Evaluation of the WOCE Volunteer Observing Ship-XBT Network in the Atlantic," J. Atmos. Ocean. Technol. **9** (3), 305–317 (1992).
14. D. N. Fox, W. J. Teague, C. N. Barron, et al., "The Modular Ocean Data Assimilation System (MODAS)," J. Atmosh. Ocean. Technol. **19** (2), 240–252 (2002).
15. V. Gouretski and K. P. Koltermann, "How Much Is the Ocean Really Warming?," Geophys. Rev. Lett. **34**, L01610 (2007) [doi: 10.1029/2006GL027834].
16. J. I. Isern-Fontanet, E. Garcia-Ladona, J. Font, et al., "Non-Gaussian Velocity Probability Density Function: An Altimetric Perspective of the Mediterranean Sea," J. Phys. Oceanogr. **36** (11), 2153–2164 (2006).
17. V. O. Ivchenko, N. C. Wells, and D. L. Aleynik, "Anomaly of Heat Content in the Northern Atlantic in the Last 7 Years: Is the Ocean Warming or Cooling?," Geophys. Rev. Lett. **33**, L22606 (2006).
18. S. M. Lasarus, C. G. Calvert, M. E. Splitt, et al., "Real-Time, High-Resolution, Space-Time Analysis of Sea Surface Temperatures from Multiple Platforms," Mon. Weather Rev. **135** (9), 3158–3173 (2007).
19. S. Levitus, T. P. Boyer, M. E. Conkright, et al., "World Ocean Database 1998," in *Introduction NOAA Atlas NESDIS 18* (U.S. Gov. Printing Office, Washington, D.C., 1998), Vol. 1.
20. S. Levitus, J. I. Antonov, T. P. Boyer, et al., "Warming of the World Ocean," Science **287**, 2225–2229 (2000).
21. S. Levitus, J. Antonov, and T. Boyer, "Warming of the World Ocean, 1995–2003," Geophys. Res. Lett. **32**, L02604 (2005) [doi: 10.1029/2004GL021592].
22. R. A. Locarnini, A. V. Mishonov, J. I. Antonov, et al., *World Ocean Atlas 2005*, Vol. 1: *Temperature*, Ed. by S. Levitus, *NOAA Atlas NESDIS 61* (U.S. Government Printing Office, Washington, DC, 2006).
23. G. A. Meyers, J. Sprintall, H. E. Phillips, et al., Design of an Ocean Temperature Observing Network in the Seas North of Australia. Part I. Tropical Ocean: Statistics. CSIRO Marine Laboratories Report. No. 204 (1989).
24. H. Phillips, R. Bailey, and G. Meyers, Design of an Ocean Temperature Observing Network in the Seas North of Australia. Part II. Tropical Ocean: Statistics. CSIRO Marine Laboratories Report. No. 211 (1990).
25. C. Stephens, J. I. Antonov, T. P. Boyer, et al., *World Ocean Atlas 2001*, Vol. 1: *Temperature*, Ed. by S. Levitus, *Atlas NESDIS 49* (U.S. Government Printing Office, Washington, D.C., 2002).
26. W. B. White, "Design of a Global Observing System for Gyre-Scale Upper Ocean Temperature Variability," Progr. Oceanogr. **36** (3), 169–217 (1995).
27. W. White and R. Bernstein, "Design of an Oceanographic Network in the Midlatitude North Pacific," J. Phys. Oceanorg. **9** (3), 592–606 (1979).
28. W. B. White, G. Meyers, and K. Hasunuma, "Space/Time Statistics of Short Term Climatic Variability in the Western North Pacific," J. Geophys. Res. **87** (C3), 1979–1989 (1982).
29. S. J. Worley, S. D. Woodruff, R. W. Reynolds, et al., "ICOADS Release 2.1 Data and Products," Int. J. Climatol. **25** (7), 823–842 (2005).